First-principles study of structure, elasticity, and electronic properties of ternary semiconductor $Al_4In_2N_6$ under high pressure*

CHEN Meijuan[1], GUO Jiaxin[1], WU Hao[1], ZHENG Xiaoran[1], MIN Nan[1], TIAN Hui[1], LI Quanjun[2], DU Shiyu[3,4,5], SHEN Longhai[1]

1.School of Science, Shenyang Ligong University, Shenyang 100159, China

2.State Key Laboratory of Superhard Materials, Jinlin University, Changchun 130012, China

3.College of Materials Science and Chemical Engineering, Harbin Engineering University, Harbin 150001, China

4.Ningbo Institute of Materials Technology and Engineering, Chinese Academy of Sciences, Ningbo 315201, China

5.School of Materials Science and Engineering, China University of Petroleum (East China), Qingdao 266580, China

Abstract

The effects of pressure on the crystal structure, elastic properties, and electronic characteristics of $Al_4In_2N_6$ are systematically studied using first-principles density functional theory. The lattice constants of $Al_4In_2N_6$ decrease with the increase of pressure, exhibiting anisotropic compression with greater compressibility along the *c*-axis. In terms of mechanical properties, the bulk modulus increases with the increase of pressure, indicating enhanced compressive resistance. Notably, the Vickers hardness decreases with the increase of pressure, indicating that high pressure can induce plastic deformation in $Al_4In_2N_6$. The calculations of elastic constants and phonon spectra confirm that $Al_4In_2N_6$ retains mechanical and dynamical stability in the pressure range of 0–30 GPa. Electronic structure calculations reveal that $Al_4In_2N_6$ possesses a direct band gap, and non-overlapping conduction and valence bands at the Fermi level. The conduction band has a higher carrier mobility than the valence band. The band gap increases almost linearly with pressure rising from 3.35 eV at 0 GPa to 4.24 eV at 30 GPa, demonstrating significant pressure-induced modulation of the electronic structure. Furthermore, the analysis of differential charge densities reveals that increasing pressure can

---

* The paper is an English translated version of the original Chinese paper published in Acta Physica Sinica. Please cite the paper as: **CHEN Meijuan, GUO Jiaxin, WU Hao, ZHENG Xiaoran, MIN Nan, TIAN Hui, LI Quanjun, DU Shiyu, SHEN Longhai, First-principles study of structure, elasticity, and electronic properties of ternary semiconductor $Al_4In_2N_6$ under high pressure.** *Acta Phys. Sin.*, 2025, 74(17): 177102. doi: 10.7498/aps.74.20250287

strengthen the Al-N and In-N bonds in $Al_4In_2N_6$ through shortened interatomic distances and stronger atomic interactions, increasing its compression resistance. In summary, this study not only deepens our understanding of the high-pressure properties of $Al_4In_2N_6$ but also provides theoretical guidance for its application in UV optoelectronics. Pressure-driven modulation of its mechanical and electronic characteristics highlights its potential in efficient high-pressure optoelectronic devices and materials.

The effects of pressure on the crystal structure, elastic properties, and electronic characteristics of $Al_4In_2N_6$ are systematically studied using first-principles density functional theory. The lattice constants of $Al_4In_2N_6$ decrease with the increase of pressure, exhibiting anisotropic compression with greater compressibility along the *c*-axis. In terms of mechanical properties, the bulk modulus increases with the increase of pressure, indicating enhanced compressive resistance. Notably, the Vickers hardness decreases with the increase of pressure, indicating that high pressure can induce plastic deformation in $Al_4In_2N_6$. The calculations of elastic constants and phonon spectra confirm that $Al_4In_2N_6$ retains mechanical and dynamical stability in the pressure range of 0–30 GPa. Electronic structure calculations reveal that $Al_4In_2N_6$ possesses a direct band gap, and non-overlapping conduction and valence bands at the Fermi level. The conduction band has a higher carrier mobility than the valence band. The band gap increases almost linearly with pressure rising from 3.35 eV at 0 GPa to 4.24 eV at 30 GPa, demonstrating significant pressure-induced modulation of the electronic structure. Furthermore, the analysis of differential charge densities reveals that increasing pressure can strengthen the Al-N and In-N bonds in $Al_4In_2N_6$ through shortened interatomic distances and stronger atomic interactions, increasing its compression resistance. In summary, this study not only deepens our understanding of the high-pressure properties of $Al_4In_2N_6$ but also provides theoretical guidance for its application in UV optoelectronics. Pressure-driven modulation of its mechanical and electronic characteristics highlights its potential in efficient high-pressure optoelectronic devices and materials.

Keywords: ternary semiconductor, high pressure, first-principles, band gap

PACS：71.20.Nr, 62.50.–p, 63.20.dk, 71.20.–b

doi: 10.7498/aps.74.20250287

cstr: 32037.14.aps.74.20250287

1. Introduction

III-V nitride semiconductor materials have attracted much attention due to their wide applications in light emitting diodes (LEDs), laser diodes (LDs), photodetectors, and distributed Bragg reflectors (DBRs)[1-5]. Among them, AlN has shown significant advantages

in ultraviolet optoelectronic devices and high temperature environment due to its wide band gap (6. 2 eV), high thermal conductivity and excellent chemical stability[6-8]. In contrast, InN has unique advantages in infrared optoelectronic devices and high-speed electronic devices due to its narrow band gap (0. 7 eV) and high carrier mobility[9,10]. However, the thermodynamic stability of InN is poor, and it is easy to decompose in high temperature environment. Its chemical stability and mechanical properties are also weak, which limits its application in extreme conditions[11,12].

The complementary characteristics of AlN and InN provide a potential for the regulation of the properties of III-V nitride semiconductor materials. Researchers aim to obtain better material properties by introducing In atoms into AlN to construct a ternary compound $Al_{1-x}In_xN$ system. The advantage of $Al_{1-x}In_xN$ material is that the incorporation of In atoms can not only adjust the lattice constant of the material, but also significantly change the size of its band gap and the[13] of its photoelectric properties, thus achieving a wide band gap coverage from infrared to ultraviolet[14-17]. For example, Chen et al.[18] successfully prepared $Al_{1-x}In_xN$ thin films by RF magnetron sputtering, and found that the band gap of Al_{1-x} In_xN decreased from 2. 95 eV to 2. 20 eV with the increase of In content. Moussa et al.[19]studied the crystal structure, electronic structure and optical properties of $Al_{1-x}In_xN$ by first principles, and found that the lattice constant decreased and the bulk modulus increased with the increase of Al content. In addition, $Al_{1-x}In_xN$ combines the high thermal stability of AlN with the high carrier mobility of InN. More importantly, the excellent performance of $Al_{1-x}In_xN$ further expands its potential in different application scenarios[20-24]. For example, Dong et al.[25] have shown that $Al_{0.83}In_{0.17}N$/GaN devices have higher sensitivity, faster response time, lower degradation and better stability than traditional AlGaN/GaN devices in aqueous solution, showing their great advantages in the field of sensors. In addition, the research of Li et al.[26] shows that the sheet resistance of high electron mobility transistors (HEMTs) composed of AlInN/GaN heterostructure is significantly reduced by 51.2% compared with that of AlGaN/GaN heterostructure, which greatly improves the current driving capability and output performance of the device. Robin Chang et al.[27] showed that $Al_{1-x}In_xN$ exhibited excellent absorption properties and high refractive index in the ultraviolet spectral range, which is suitable for photoelectric detection devices. In addition, Borovac et al.[28] reported that AlInN materials also have excellent high temperature stability (up to 950-1050 ℃), indicating that Al-In-N materials have broad application prospects in the field of high-performance electronic devices, further broadening their application scope under extreme conditions.

Mechanical properties play an important role in material design and optimization, especially under stress and pressure. The mechanical response of materials determines their stability and application prospects. It has been shown that the mechanical properties of nitride semiconductors, such as elastic modulus and hardness, play a vital role in the optimization of

material properties. For example, Yonenaga et al.[29] measured indium nitride (InN) thin films grown on sapphire substrates by nanoindentation. The Young's modulus is (184±5) GPa, and the bulk modulus and shear modulus are (99±3) GPa and (77±2) GPa, respectively. The mechanical properties of InN thin films are closely related to their crystal structure, which provides an important basis for understanding the mechanical behavior of nitride semiconductor materials. Tan et al.[30]studied the mechanical properties of AlN by first-principles calculations, and found that the WZ structure of AlN is superior to the ZB structure in compression resistance, shear resistance and elastic anisotropy, and both of them show brittleness.

Pressure, as an important external regulatory means, can alter atomic spacing, chemical bonding characteristics, and electron cloud distribution [31], thereby modifying the crystal structure [32], electronic properties [33], and optical properties [34] of materials. Although Al-In-N system materials exhibit broad application potential [35], current research primarily focuses on optimizing performance by adjusting the composition ratio of Al and In, making pressure regulation a topic worthy of further exploration. Robin Chang et al. [36] used USPEX structure searching and VASP (Vienna *ab initio* simulation package) calculations in 2016 to discover that among various Al-In-N systems, the orthorhombic phase $Al_4In_2N_6$ is the thermodynamically most stable structure under ambient pressure, with a formation enthalpy of -0.0114 eV/block. Therefore, based on this finding, the crystal structure, mechanical properties and electronic properties of $Al_4In_2N_6$ under different pressures were systematically studied in this paper. The effects of pressure on the lattice constants and elastic constants of $Al_4In_2N_6$ are analyzed, and their anisotropy is discussed. The dynamic stability of $Al_4In_2N_6$ in the pressure range of 0–30 GPa is verified by phonon spectrum calculation. The change of band gap of $Al_4In_2N_6$ under pressure was explored, and its variation was systematically analyzed. This study not only provides a theoretical basis for optimizing the properties of $Al_4In_2N_6$ materials, but also points out the direction for the design and development of new and efficient devices.

2. Details of calculation

Density functional theory (DFT) calculations were performed using the VASP code, corrected for the interaction and correlation potential between electrons by the Perdew-Burke-Ernzerhof (PBE) method in the generalized gradient approximation (GGA)[42,43]. The total energy convergence criterion during optimization was 1×10^{-6} eV/atom, and the convergence criterion for force was 1×10^{-4} eV/Å. The plane-wave cutoff energy was set to 520 eV, and a $5 \times 9 \times 10$ Monkhorst Pack grid[44] was used to sample the *k* points in the Brillouin zone. Phonon spectra were calculated using the PHONOPY[45,46] package with a supercell setting of $2 \times 2 \times 2$. In this study, the band structure of the $Al_4In_2N_6$ primitive cell was calculated using the HSE06 hybrid functional (mixing parameter $\alpha = 0.25$)[47], and self-consistent iterative

calculations were performed on a 7 × 7 × 8 *k* point grid. This method combines the exchange conditions of Hartree-Fock and DFT, which can effectively describe the electronic structure and dynamic behavior of materials, and improve the accuracy of band gap calculation[48-50].

3. Results and Discussion

3.1 Crystal structure

The optimized unit cell structure of $Al_4In_2N_6$ at 0 GPa is shown in Fig. 1. The crystal structure of $Al_4In_2N_6$ is orthorhombic phase, belonging to the space group $Cmc2_1$ (No.36). The unit cell of $Al_4In_2N_6$ contains 24 atoms, including 8 equivalent Al atoms with Wyckoff positions of 8*b* (0.329, 0.664, 0.560) and 4 equivalent In atoms with Wyckoff positions of 4*a* (0, 0.678, 0.556); 8 equivalent N_1 atoms 8*b* (0.815, 0.852, 0.424) and 4 equivalent N_2 atoms 4*a* (0, 0.298, 0.475).

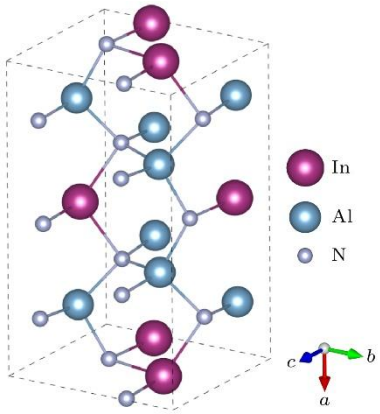

Figure 1. Crystal structure of $Al_4In_2N_6$.

In order to study the effect of pressure on the crystal structure of $Al_4In_2N_6$, the lattice constants *a*,*b*,*c* of $Al_4In_2N_6$ at 0–30 GPa were calculated, and the results are listed in Tab. 1. It can be seen from the Tab. 1 that the lattice constant of $Al_4In_2N_6$ decreases along the *a*,*b* and *c* axes with the increase of pressure.

Table 1. Lattice parameters of $Al_4In_2N_6$ under different pressures.

Pressure/GPa	*a*/Å	*b*/Å	*c*/Å
0	9.832	5.654	5.250
5	9.749	5.603	5.195
10	9.669	5.557	5.149
15	9.600	5.516	5.107
20	9.535	5.478	5.068
25	9.477	5.445	5.032
30	9.422	5.413	4.999

Fig. 2 gives the calculated relative lattice constants (a/a_0,b/b_0,c/c_0) and relative volumes (V/V_0) of $Al_4In_2N_6$ as a function of pressure. In the given pressure range (0–30 GPa), the change of the lattice constant *c* of $Al_4In_2N_6$ is more significant than that of *a* and *b*, which indicates that the material. This phenomenon may be related to the weaker bonding along the *c* axis, making the compression more pronounced in this direction. The relative volume (V/V_0) of $Al_4In_2N_6$ decreases by 12.6% in the pressure range of 0–30 GPa, which indicates that the external pressure has a significant effect on its crystal structure. In addition, with the increase of pressure, the change of V/V_0 tends to be stable, which may be related to the strength of crystal chemical bond under high pressure.

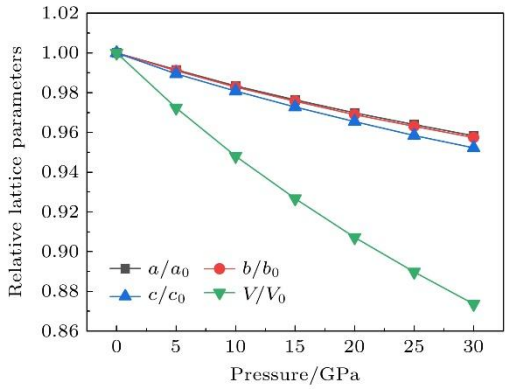

Figure 2. Pressure dependence of relative lattice parameters and relative unit cell volume for $Al_4In_2N_6$.

In order to analyze the bonding characteristics and charge transfer under high pressure, we calculated the differential charge density of $Al_4In_2N_6$ at 0, 15 and 30 GPa Fig. 3. In the Fig. 3,

yellow means gain of electrons and cyan means loss of electrons. From the Fig. 3(a), it can be seen that N atom has a strong ability to get electrons, Al atom has a strong ability to lose electrons, and In atom is relatively isolated. Al atom and N atom form a strong chemical bond, while In atom and N atom form a relatively weak chemical bond. With the increase of pressure, the strength of Al-N bond increases gradually, and the strength of In-N bond also increases to a certain extent. When the pressure reaches 30 GPa, both Al-N and In-N bonds increase significantly. At the same time, the charge distribution gradually transits from irregular anisotropy to ellipsoidal distribution, and the polarity decreases. This is because under high pressure, the distance between atoms is shortened and the interaction force between atoms is enhanced, which makes it more difficult for the crystal to be further compressed.

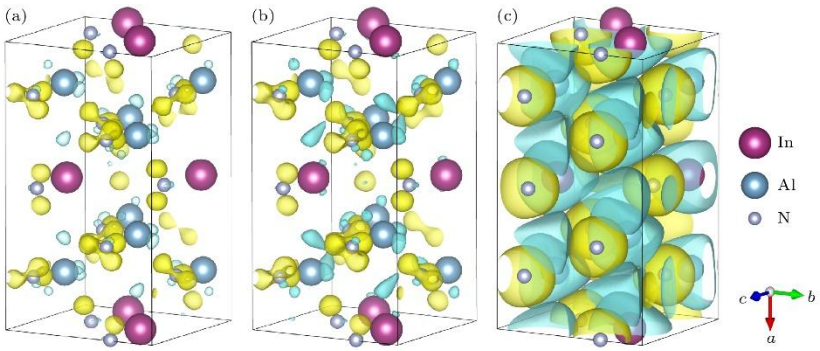

Figure 3. Differential charge density of $Al_4In_2N_6$ under different pressures: (a) 0 GPa; (b) 15 GPa; (c) 30 GPa.

In order to determine the dynamical stability of $Al_4In_2N_6$ under pressure, we calculated the phonon dispersion curves (e.g., Fig. 4) at 0, 10, 20 and 30 GPa. From the Fig. 4, it can be seen that there is no imaginary frequency in the whole Brillouin zone, and the curve gradually spreads and becomes looser with the increase of pressure, indicating that the $Al_4In_2N_6$ phase is dynamically stable at both normal and high pressures. This is consistent with the kinetic stability of Al-In-N system with different ratios in all metastable phases studied by Robin Chang et al.[51].

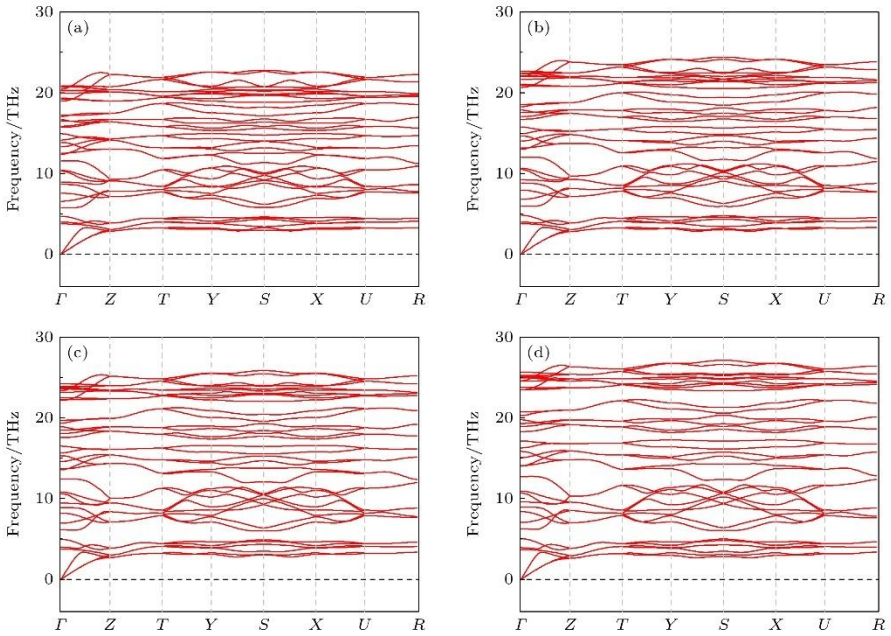

Figure 4. Phonon dispersion curves for $Al_4In_2N_6$ at different pressures: (a) 0 GPa; (b) 10 GPa; (c) 20 GPa; (d) 30 GPa.

3.2 Mechanical property

The elastic constants of materials are the key physical parameters to describe the mechanical response of crystals under external stress, which are essential for further understanding and predicting the mechanical properties of solid materials. The systematic study of elastic constants of materials can provide scientific basis and theoretical support for the design and optimization of materials and the development of new materials. In the orthorhombic system, the material has significant anisotropic characteristics due to its different elastic properties in three mutually perpendicular axes. The elastic constant matrix of the orthorhombic system is a diagonally symmetric 6 × 6 matrix containing nine independent elastic constants:C_{11},C_{22},C_{33},C_{44},C_{55},C_{66},C_{12},C_{13}, and C_{23}. The calculated elastic constants of $Al_4In_2N_6$ in the pressure range of 0–30 GPa are listed in Tab. 2.

Table 2. Elastic constant of $Al_4In_2N_6$ under 0–30 GPa pressures.

Pressure/GPa	C_{11}/GPa	C_{12}/GPa	C_{13}/GPa	C_{22}/GPa	C_{23}/GPa	C_{33}/GPa	C_{44}/GPa	C_{55}/GPa	C_{66}/GPa
0	318.606	113.886	89.017	305.200	92.444	311.408	84.739	84.903	95.602
5	330.169	126.317	103.218	327.053	105.181	326.999	86.887	88.385	96.321
10	340.077	143.266	118.822	337.579	124.623	338.138	85.186	87.028	94.397
15	359.171	163.187	130.986	352.270	135.623	357.799	88.682	87.873	95.539
20	375.952	175.971	146.621	363.912	151.179	361.684	89.566	86.445	93.548
25	389.382	192.252	161.374	370.366	171.460	363.533	88.451	87.052	91.683
30	402.037	207.158	171.490	379.130	181.476	381.927	86.653	84.002	90.021

According to the mechanical stability criterion[52] proposed by Born for the orthorhombic system, the following conditions should be satisfied:

$$\begin{cases} C_{11} > 0;\ C_{11}C_{12} > C_{12}^2, \\ C_{11}C_{22}C_{33} + 2C_{12}C_{13}C_{23} - C_{11}C_{23}^2 \\ \quad - C_{22}C_{13}^2 - C_{33}C_{12}^2 > 0, \\ C_{44} > 0;\ C_{55} > 0;\ C_{66} > 0. \end{cases} \tag{1}$$

According to the mechanical stability criterion of orthorhombic system, the of $Al_4In_2N_6$ satisfies the mechanical stability criterion.

The elastic constants C_{11},C_{22}, and C_{33} correspond to the tensile or compressive stiffness in the three orthogonal directions of the *a*,*b*, and *c* axes of the lattice, respectively. It can be seen from Fig. 5(a) that C_{11},C_{22},C_{33} increase gradually with the increase of pressure, indicating that the stiffness of the material in these directions increases with the increase of pressure. In the pressure range of 0–30 GPa, the increase of C_{11} is larger than that of C_{22} and C_{33}. The results show that the ability of $Al_4In_2N_6$ to resist tension or compression in the direction of *a* axis is more obvious. This phenomenon is usually associated with the densification of crystal structures at high pressure, that is, at higher pressures, the atomic spacing decreases, resulting in an increase in the stiffness of the material. C_{12}, C_{13} and C_{23} represent the coupling effect between the two orthogonal axis directions. Fig. 5(a) shows that they also increase with the increase of pressure. The value of C_{12} is significantly higher than that of C_{13} and C_{23}, indicating that the coupling effect of *x* and *y* directions is stronger. In addition,C_{44},C_{55},C_{66} represent the shear stiffness of the material in the *xy*, *yz*, and *zx* planes, respectively. It can be seen from Fig. 5(a) that C_{44}, C_{55}, C_{66} have very similar change trends with the increase of pressure, and the change range is relatively small. This means that the shear stiffness of the material is less sensitive to pressure, indicating that the mechanical properties of $Al_4In_2N_6$ in these directions remain stable.

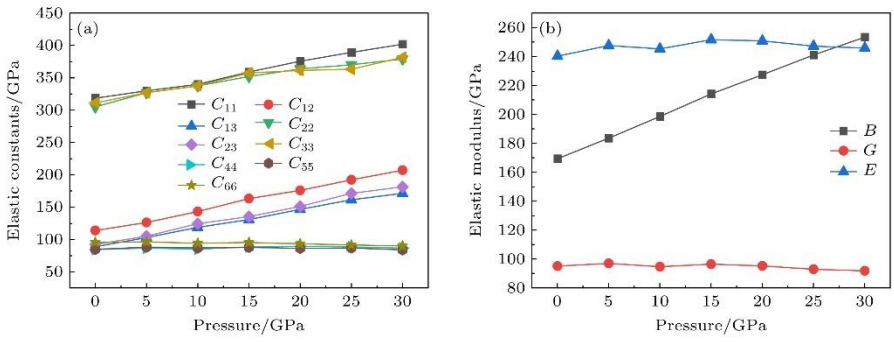

Figure 5. The elastic constants (a) and elastic modulus (b) of $Al_4In_2N_6$ change with pressure.

Bulk modulus (*B*), shear modulus (*G*) and Young's modulus (*E*) can measure the resistance to fracture, plastic deformation and stiffness of materials, which is of great significance for understanding the solid state properties of materials. The elastic moduli (*B*,*E*,*G*) of $Al_4In_2N_6$

ternary compounds were calculated by the Voigt-Reuss-Hill (VRH) approximation method for[53-55]:

$$B_{\mathrm{V}} = \frac{1}{9}[(C_{11} + C_{22} + C_{33}) + 2(C_{12} + C_{13} + C_{23})], \tag{2}$$

$$\begin{aligned} B_{\mathrm{R}} = \Delta[&C_{11}(C_{22} + C_{33} - 2C_{23}) + C_{22}(C_{33} - 2C_{13}) \\ &- 2C_{33}C_{12} + C_{12}(2C_{23} - C_{12}) \\ &+ C_{13}(2C_{12} - C_{13}) + C_{23}(2C_{13} - C_{23})]^{-1}, \end{aligned} \tag{3}$$

$$\begin{aligned} G_{\mathrm{V}} = (1/15)\big[&(C_{11} + C_{22} + C_{33}) + 3(C_{44} + C_{55} \\ &+ C_{66}) - (C_{12} + C_{23} + C_{13})\big], \end{aligned} \tag{4}$$

$$\begin{aligned} G_{\mathrm{R}} = 15\big\{&4[C_{11}(C_{22} + C_{33} + C_{23}) + C_{22}(C_{33} + C_{13}) \\ &+ C_{33}C_{12} - C_{12}(C_{23} + C_{12}) - C_{13}(C_{12} + C_{13}) \\ &- C_{23}(C_{13} + C_{23})]/\Delta + 3[(1/C_{44}) + (1/C_{55}) \\ &+ (1/C_{66})]\big\}^{-1}, \end{aligned} \tag{5}$$

Among

$$\begin{aligned} \Delta = &C_{13}\left(C_{12}C_{23} - C_{13}C_{22}\right) + C_{23}\left(C_{12}C_{13}\right. \\ &\left. - C_{23}C_{11}\right) + C_{33}\left(C_{11}C_{22} + C_{12}^{2}\right), \end{aligned} \tag{6}$$

Where B_{V} and B_{R} are the maximum and minimum values of the bulk modulus B of $Al_4In_2N_6$, respectively, and G_{V} and G_{R} are the maximum and minimum values of the shear modulus G of $Al_4In_2N_6$, respectively.

Taking the arithmetic average of the two methods, one obtains

$$B = 1/2(B_{\mathrm{R}} + B_{\mathrm{V}}), \tag{7}$$

$$G = 1/2(G_{\mathrm{R}} + G_{\mathrm{V}}). \tag{8}$$

According to the calculated bulk modulus B and shear modulus G, we can also calculate the Young's modulus E, Poisson's ratio μ[56], Vickers hardness H_{V}[57] calculation formula, and the results are listed in Tab. 3.

Table 3. The elastic modulus (*B*, *G*, *E*, *B*/*G*), hardness (H_V), and Poisson's ratio (μ) of $Al_4In_2N_6$ under pressures of 0–30 GPa.

Pressure/GPa	*B*/GPa	*E*/GPa	*G*/GPa	*B*/*G*	μ	H_V/GPa
0	169.443	240.336	95.099	1.782	0.264	11.998
5	183.649	247.651	97.099	1.891	0.275	11.377
10	198.718	245.38	94.800	2.096	0.294	9.952
15	214.192	251.75	96.522	2.219	0.304	9.447
20	227.465	250.967	95.344	2.386	0.316	8.625
25	241.177	247.277	93.023	2.593	0.329	7.711
30	253.426	245.888	91.866	2.759	0.338	7.123

$$E = 9BG/(3B + G), \tag{9}$$

$$\mu = (3B - 2G)/(6B + 2G), \tag{10}$$

$$H_{\mathrm{V}} = 0.92(G/B)^{1.137}G^{0.708}. \tag{11}$$

According to the above formula, we calculate the elastic modulus (*B*,*G*,*E*), Poisson's ratio μ, Vickers hardness H_V of $Al_4In_2N_6$ as listed in Tab. 3. It can be seen from Fig. 5(b) that the bulk modulus *B* increases linearly with the increase of pressure, from about 169 GPa to nearly 220 GPa. This indicates that $Al_4In_2N_6$ exhibits greater resistance to compression at higher pressures. The shear modulus *G* changes gently in the whole pressure range, indicating that the shear stiffness of $Al_4In_2N_6$ material is almost unchanged under different pressures. Young's modulus *E* fluctuates slightly with the increase of pressure and remains in the range of 240–250 GPa, indicating that the axial stiffness of $Al_4In_2N_6$ material increases slightly under high pressure, but the overall change is small.

Poisson's ratio μ is the ratio of transverse strain to longitudinal strain under stress, which is generally used to measure the stability of crystal against shear strain. Frantsevich et al.[56]proposed a criterion to judge the toughness and brittleness of materials by Poisson's ratio, that is, when the Poisson's ratio of a material is greater than 0.26, the material is considered to be tough, otherwise it is brittle. Poisson's ratio can also be used to emphasize the strength of covalent bonds. If the Poisson's ratio of the alloy is less than 0.26, it has a covalent bond. From the Tab. 3, it can be observed that the Poisson's ratio of $Al_4In_2N_6$ is greater than 0.26, which indicates that $Al_4In_2N_6$ materials are ductile and increase with the increase of pressure. It is generally believed that materials can produce larger transverse deformation when subjected to tension, show better stress dispersion ability, and can undergo greater plastic deformation before fracture, thus absorbing more energy. Therefore, $Al_4In_2N_6$ material has better fracture resistance.

Hardness is one of the key mechanical properties of materials, especially in evaluating the deformation resistance and stability of materials under different external conditions. Under high pressure environment, the change of hardness can reveal the deformation mechanism,

potential transformation behavior, plastic and elastic characteristics of materials. From the Tab. 3, it can be observed that the Vickers hardness of $Al_4In_2N_6$ material decreases gradually with the increase of pressure, and the Vickers hardness decreases from 11. 998 GPa to 7. 123 GPa in the range of 0–30 GPa, which indicates that $Al_4In_2N_6$ material becomes soft gradually during the compression process. When the pressure increases to 30 GPa, the hardness of the material decreases significantly, which may indicate that the $Al_4In_2N_6$ material has entered the plastic deformation stage.

Understanding elastic anisotropy is a necessary condition for improving mechanical durability. As mentioned earlier, the $Al_4In_2N_6$ compound exhibits significant elastic anisotropy. In order to further understand the effect of pressure on the anisotropy of $Al_4In_2N_6$, the three-dimensional surface plots of bulk modulus, shear modulus and Young's modulus of $Al_4In_2N_6$ at 0, 10, 20 and 30 GPa are plotted, and the results are shown in Fig. 6. In Fig. 6, the different color areas represent the modulus, [001], [100], [010] indicate the direction of the crystal axis, and the degree of deviation of the three-dimensional curved surface from the sphere reflects the degree of anisotropy of the material. For the convenience of observation and analysis, the Fig. 6(a) color scale of bulk modulus is 160–210 GPa, the Fig. 6(b)–(d) color scale is 160–280 GPa, the shear modulus color scale is 85-100 GPa, and the Young's modulus color scale is 230–280 GPa, which can more intuitively reveal the trend and anisotropy evolution characteristics of modulus with pressure.

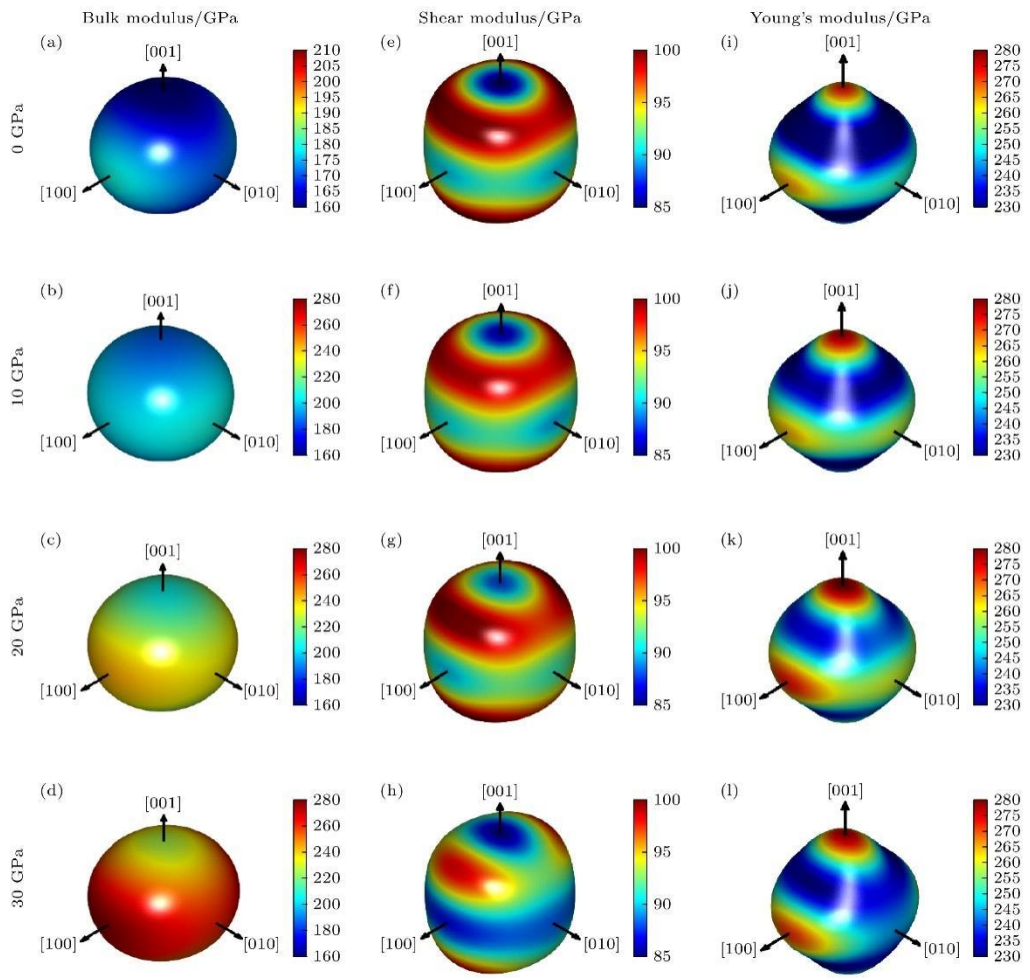

Figure 6. The 3D plot of bulk modulus ((a)–(d)), shear modulus ((e)–(h)), and Young's modulus ((i)–(l)) of $Al_4In_2N_6$ under pressures of 0, 10, 20, and 30 GPa.

From the Fig. 6(a)–(d), it can be observed that the bulk modulus of $Al_4In_2N_6$ changes from dark blue to yellow in [001] crystal direction, from cyan to dark red in [100] direction, and from light blue to red in [010] direction with the increase of applied pressure. It can be concluded that the color change and growth rate are different in each direction, but the overall compression resistance of the material is significantly enhanced under high pressure. The bulk modulus distribution of Fig. 6(a)–(d) is almost spherical, indicating that the bulk modulus anisotropy of $Al_4In_2N_6$ changes little in the pressure range of 0–30 GPa.

In contrast, the shear modulus Fig. 6(e)–(h) shows a significant directional difference. At 0 GPa Fig. 6(e), the [001] direction is the weakest shear modulus region, showing a blue low band. With the increase of pressure, this direction still maintains a relatively low value, but the difference between the shear modulus of this direction and that of [100] and [010] directions gradually decreases, indicating that the anisotropy of $Al_4In_2N_6$ is slightly weakened.

Young's modulus Fig. 6(i)–(l), it is clear that Young's modulus increases with pressure in the [100] direction. At 0 GPa Fig. 6(i), the [001] direction corresponds to the highest Young's

modulus and changes little with the increase of pressure, while the [100] and [010] directions are relatively low, and the [010] direction increases first and then decreases with the increase of pressure. Fig. 6(i)–(l) From the degree of spherical deviation, it can be seen that the anisotropy of $Al_4In_2N_6$ material changes little with the increase of pressure.

On the whole, the bulk modulus of $Al_4In_2N_6$ increases gradually with the increase of pressure, while the shear modulus and Young's modulus show more significant directional evolution. The shear modulus and Young's modulus of $Al_4In_2N_6$.With the increase of pressure, the anisotropy of the material changes little as a whole, but the difference is obvious in different crystal directions, which indicates that the mechanical properties of $Al_4In_2N_6$ have strong directional changes. This provides an important theoretical basis for the potential of $Al_4In_2N_6$ in high pressure applications, especially in areas requiring high elastic modulus and deformation resistance (such as high pressure equipment or semiconductor applications), $Al_4In_2N_6$ may show more excellent performance.

3.3 Electronic properties

Band structure is essential for understanding the physical properties of materials. In order to explore the effect of pressure on the electronic properties of $Al_4In_2N_6$, the band structures of $Al_4In_2N_6$ at 0, 5, 10, 15, 20, 25 and 30 GPa were calculated and discussed, and the results are shown in Fig. 7.

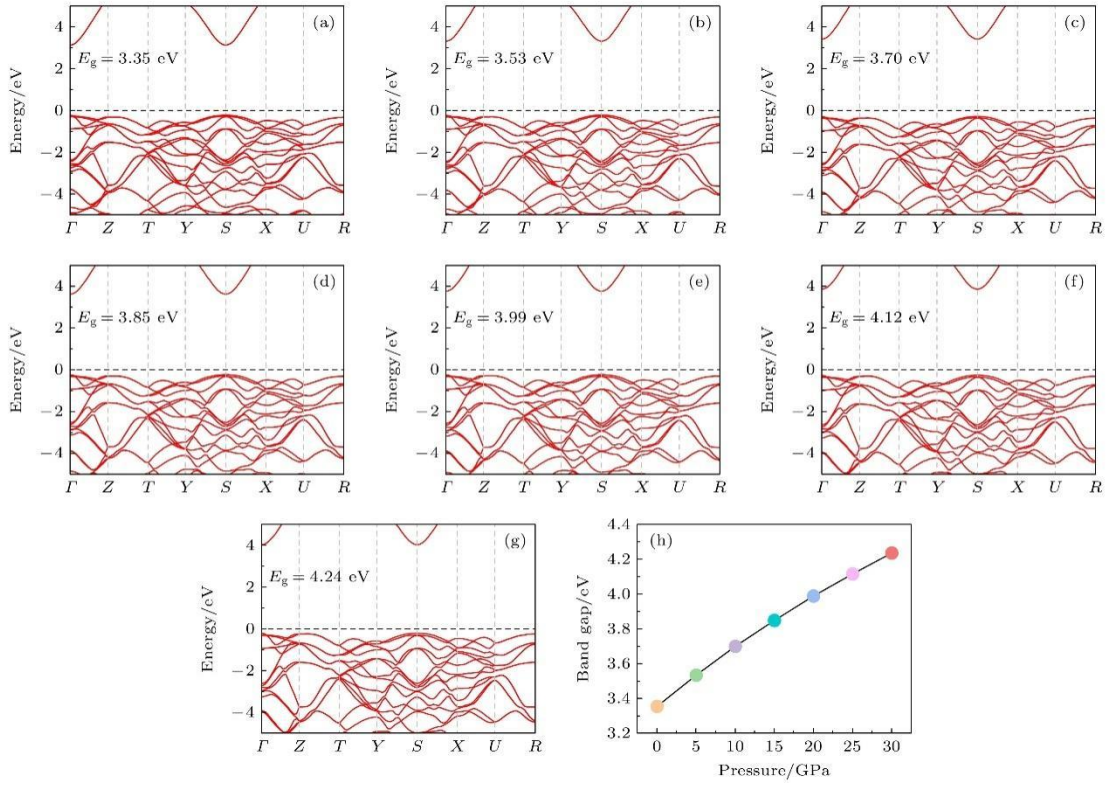

Figure 7. The band structures of $Al_4In_2N_6$ at (a) 0 GPa, (b) 5 GPa, (c) 10 GPa, (d) 15 GPa, (e) 20 GPa, (f) 25 GPa, (g) 30 GPa, and (h) the variation trend of the band gap with pressure.

From the Fig. 7(a)–(g), it can be observed that in the given pressure range, there is no overlap between the conduction band and the valence band of $Al_4In_2N_6$ at the Fermi level, and there is a band gap near the Fermi level. The minimum of the conduction band and the maximum of the valence band are located at the same *k* point (*Γ* point in the Brillouin zone, that is, $k = 0$), which indicates that $Al_4In_2N_6$ is a semiconductor material with a direct band gap. In addition, the curvature of the dispersion curve at the bottom of the conduction band is always greater than that at the top of the valence band, which means that the mobility of electrons is higher than that of holes, and the effective mass of electrons is smaller. These characteristics have an important impact on the migration behavior of electrons and holes in $Al_4In_2N_6$ materials.

Fig. 7(h) gives the relationship between the band gap of $Al_4In_2N_6$ and pressure. It can be observed that the band gap of $Al_4In_2N_6$ increases linearly with the increase of pressure, from 3. 35 eV at 0 GPa to 4. 24 eV at 30 GPa, and the corresponding absorption photon wavelength decreases from 370 nm (near ultraviolet region of ultraviolet spectrum) to 292 nm (middle ultraviolet region of ultraviolet spectrum). At low pressure (0 GPa), the material has a small band gap and a relatively small energy difference between the bottom of the conduction band and the top of the valence band, which is more suitable for absorbing or emitting low-energy photons, so that the material can effectively absorb or emit near-ultraviolet light. This property indicates that it is suitable for emitters or detectors of low energy ultraviolet light. At higher pressure (30 GPa), the band gap increases to 4. 24 eV, and the optical absorption range of the material enters the mid-ultraviolet region[58]. Therefore, under high pressure, $Al_4In_2N_6$ can absorb higher energy photons, and the absorption wavelength gradually shortens from the near-ultraviolet region to the mid-ultraviolet region.

The study of the density of States (DOS) is essential for understanding the bonding characteristics and electrical behavior of crystals. We further calculated the density of States of $Al_4In_2N_6$ under different pressures. The results are shown in the Fig. 8. The horizontal axis in the Fig. 8 represents the energy (unit: eV), and the vertical axis represents the density of States (unit: States/eV). The range of density of States near the Fermi level is selected from –6 to 16 eV, and the $E = 0$ eV marked by the dotted line is the Fermi level. At the Fermi level, the value of the density of States is zero, indicating that $Al_4In_2N_6$ has semiconductor characteristics. By analyzing the total density of States (TDOS), it is found that the total density of States of the material is mainly contributed by Al-p, In-p and N-p orbitals. Further study shows that the conduction near the Fermi level is mainly contributed by the p orbital electrons of Al and In atoms, and Al-p and In-p are the main factors affecting the electronic conduction behavior of $Al_4In_2N_6$. Al-s, In-s and N-s also contribute to the density of States near the Fermi level, but the overall effect is small.

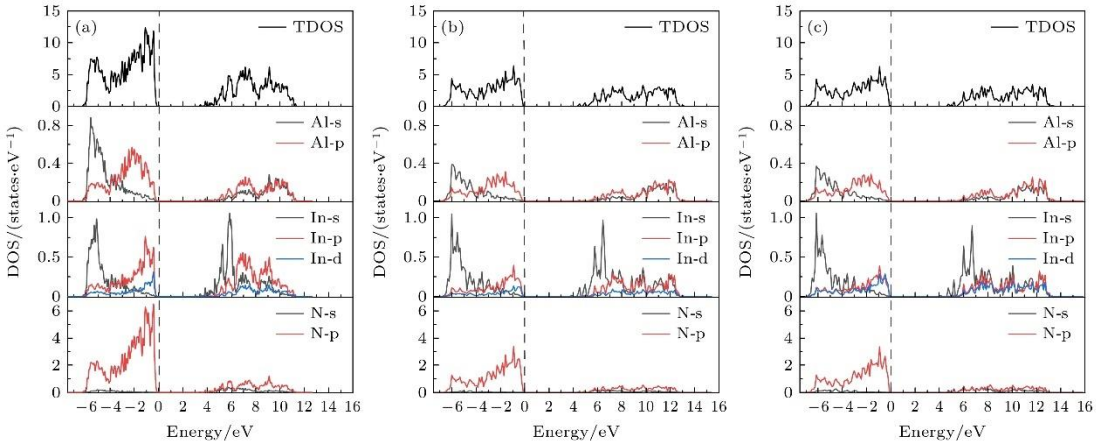

Figure 8. The total density of states and partial density of states of $Al_4In_2N_6$ at (a) 0, (b) 20, and (c) 30 GPa.

With the increase of pressure, the conduction band gradually shifts away from the Fermi level, and the density of States in the energy range of 4–10 eV decreases significantly. It can be seen from the Fig. 8(a) and Fig. 8(b) that in the pressure range of 0–20 GPa, the density of States decreases significantly, compared with the pressure range of 20–30 GPa, the change of density of States is not obvious, because at lower pressures, the compression of interatomic distance is more significant, which leads to a greater change in bonding state, thus causing a significant change in the density of States. However, when the pressure is further increased to 20–30 GPa, the interatomic force increases, the material becomes difficult to compress, and the change of bonding state tends to be flat, so the change of density of States is relatively small. In addition, with the continuous increase of pressure, the distance between atoms is further reduced, and the charge distribution is gradually delocalized. This phenomenon indicates the redistribution of electronic structure and the tendency of interaction enhancement under high pressure.

4. Conclusion

In this study, the structural, mechanical and electronic properties of $Al_4In_2N_6$ under different pressures were systematically analyzed by first-principles calculations, and the significant control effect of pressure on its properties was revealed. The lattice compression and the change of elastic constants show that the material has good mechanical stability and resistance to deformation under high pressure. Electronic structure calculations show that $Al_4In_2N_6$ is a direct band gap semiconductor, and its band gap increases linearly with pressure, which makes it have the tunable optical response characteristics required by ultraviolet optoelectronic devices. In addition, the change of density of States under high pressure further reveals the regulation mechanism of chemical bond properties. This study not only deepens the understanding of the high-pressure physical properties of $Al_4In_2N_6$, but also provides theoretical guidance for its practical application in the field of ultraviolet optoelectronics.

Future research can be combined with experiments to verify the stability and functional properties of the material under extreme conditions, and provide support for the development of new optoelectronic devices.

References

[1] Liu B, Chen D, Lu H, Tao T, Zhuang Z, Shao Z, Xu W, Ge H, Zhi T, Ren F, Ye J, Xie Z, Zhang R 2020 Adv. Mater. 32 1904354

[2] Hahn C, Zhang Z, Fu A, Wu C H, Hwang Y J, Gargas D J, Yang P 2011 ACS Nano 5 3970

[3] Yu J, Wang L, Hao Z, Luo Y, Sun C, Wang J, Han Y, Xiong B, Li H 2020 Adv. Mater. 32 1903407

[4] Chen K, Kapadia R, Harker A, Desai S, Javey A 2016 Nat. Commun. 7 10502

[5] Qiu P, Liu H, Zhu X L, Tian F, Du M C, Qiu H Y, Chen G L, Hu Y Y, Kong D L, Yang J, Wei H Y, Peng M Z, Zheng X H 2024 Acta Phys. Sin. 73 038102

[6] Manjón F J, Errandonea D, Garro N, Romero A H, Serrano J, Kuball M 2007 Phys. Status Solidi B 244 42

[7] E Abid A, Bensalem R, Sealy B J 1986 J. Mater. Sci. 21 1301

[8] Yu R, Liu G, Wang G, Chen C, Xu M, Zhou H, Wang T, Yu J, Zhao G, Zhang L 2021 J. Mater. Chem. C 9 1852

[9] Ibáñez J, Segura A, García-Domene B, Oliva R, Manjón F J, Yamaguchi T, Nanishi Y, Artús L 2012 Phys. Rev. B 86 035210

[10] Khan N, Sedhain A, Li J, Lin J Y, Jiang H X 2008 Appl. Phys. Lett. 92 172101

[11] Davydov V Y, Klochikhin A, Seisyan R, Emtsev V, Ivanov S, Bechstedt F, Furthmüller J, Harima H, Mudryi A, Aderhold J 2002 Phys. Status Solidi B 229 r1

[12] Tansley T L, Foley C P 1986 J. Appl. Phys. 59 3241

[13] Liu X K, Lin Z C, Lin Y H, Chen J J, Zou P, Zhou J, Li B, Shen L H, Zhu D L, Liu Q, Yu W J, Li X H, Zhu H, Wang X Z, Huang S W 2023 Chin. Phys. B 32 117701

[14] Wu J, Walukiewicz W, Yu K M, Ager J W, Haller E E, Lu H, Schaff W J, Saito Y, Nanishi Y 2002 Appl. Phys. Lett. 80 3967

[15] Beladjal K, Kadri A, Zitouni K, Mimouni K 2021 Superlattices Microstruct. 155 106901

[16] Guo Q G Q, Yoshida A Y A 1994 Jpn. J. Appl. Phys. 33 2453

[17] Zhao F, Yao G R, Song J J, Ding B B, Xiong J Y, Su C, Zheng S W, Zhang T, Fan G H 2013 Chin. Phys. B 22 058503

[18] Chen J J, Shen L H, Qi D L, Wu L J, Li X, Song J Y, Zhang X L 2022 Ceram. Int. 48 2802

[19] Moussa R, Abdiche A, Khenata R, Wang X, Varshney D, Sun X W, Omran S B, Bouhemadou A, Rai D 2018 J. Phys. Chem. Solids 119 36

[20] Mao W, Zhang J C, Xue J S, Hao Y, Ma X H, Wang C, Liu H X, Xu S R, Yang L A, Bi Z W, Liang X Z, Zhang J F, Kuang X W 2010 Chin. Phys. Lett. 27 128501

[21] Wen X X, Yang X D, He M, Li Y, Wang G, Lu P Y, Qian W N, Li Y, Zhang W W, Wu W B, Chen F S, Ding L Z 2012 Chin. Phys. Lett. 29 097304

[22] Zhang X F, Wang L, Liu J, Wei L, Xu J 2013 Chin. Phys. B 22 017202

[23] Han T C, Zhao H D, Yang L, Wang Y 2017 Chin. Phys. B 26 107301

[24]Zhan X M, Hao M L, Wang Q, Li W, Xiao H L, Feng C, Jiang L J, Wang C M, Wang X L, Wang Z G 2017 Chin. Phys. Lett. 34 047301

[25] Dong Y, Son D H, Dai Q, Lee J H, Won C H, Kim J G, Chen D, Lee J H, Lu H, Zhang R, Zheng Y 2018 Sensors 18 1314

[26] Li A, Wang C, Xu S, Zheng X, He Y, Ma X, Lu X, Zhang J, Liu K, Zhao Y Hao Y 2021 Appl. Phys. Lett. 119 122104

[27] Robin Chang Y H, Yoon T L, Lim T L 2016 Curr. Appl. Phys. 16 1277

[28] Borovac D, Sun W, Song R, Wierer J J, Tansu N 2020 J. Cryst. Growth 533 125469

[29] Yonenaga I, Ohkubo Y, Deura M, Kutsukake K, Tokumoto Y, Ohno Y, Yoshikawa A, Wang X Q 2015 AIP Adv. 5 077131

[30] Tan X, Xin Z Y, Liu X J, Mu Q G 2013 Adv. Mater. Res. 82-822 841

[31] Chen M, Guo G C, He L 2010 J. Phys. Condens. Matter 22 445501

[32] Al-Khatatbeh Y, Lee K K M, Kiefer B 2009 Phys. Rev. B 79 134114

[33] Man X X, Gong B C, Sun P H, Liu K, Lu Z Y 2022 Phys. Rev. B 106 035136

[34] Yu F, Liu Y 2019 Computation 7 57

[35] Velpula R T, Jain B, Philip M R, Nguyen H D, Wang R, Nguyen H P T 2020 Sci. Rep. 10 2547

[36] Robin Chang Y H, Yoon T L, Lim T L, Rakitin M 2016 J. Alloys Compd. 682 338

[37] Glass C W, Oganov A R, Hansen N 2006 Comput. Phys. Commun. 175 713

[38] Oganov A R, Lyakhov A O, Valle M 2011 Acc. Chem. Res. 44 227

[39] Lyakhov A O, Oganov A R, Stokes H T, Zhu Q 2013 Comput. Phys. Commun. 184 1172

[40] Kresse G, Furthmüller J 1996 Phys. Rev. B 54 11169

[41] Kresse G, Furthmüller J 1996 Comput. Mater. Sci. 6 15

[42] Blöchl P E 1994 Phys. Rev. B 50 17953

[43] Wu Z, Cohen R E 2006 Phys. Rev. B 73 235116

[44] Monkhorst H J, Pack J D 1976 Phys. Rev. B 13 5188

[45] Togo A, Oba F, Tanaka I 2008 Phys. Rev. B 78 134106

[46] Togo A, Tanaka I 2015 Scr. Mater. 108 1

[47] Heyd J, Scuseria G E, Ernzerhof M 2003 J. Chem. Phys. 118 8207

[48] Muscat J, Wander A, Harrison N M 2001 Chem. Phys. Lett. 342 397

[49] Garza A J, Scuseria G E 2016 J. Phys. Chem. Lett. 7 4165

[50] Sugita Y, Miyake T, Motome Y 2018 Phys. Rev. B 97 035125

[51] Robin Chang Y H, Yoon T L, Lim T L, Tuh M H 2017 J. Alloys Compd. 704 160

[52] Mouhat F, Coudert F X 2014 Phys. Rev. B 90 224104

[53] Voigt W 1889 Ann. Phys. 274 573

[54] Reuss A 1929 ZAMM - J. Appl. Math. Mech. Z. Für Angew. Math. Mech. 9 49

[55] Hill R 1952 Proc. Phys. Soc. London, Sect. A 65 349

[56] Frantsevich I N, Voronov F F and Bokuta S A 1983 Elastic Constants and Elastic Moduli of Metals and Insulators Handbook (Kiev: Naukova Dumka) pp60–180

[57] Tian Y, Xu B, Zhao Z 2012 Int. J. Refract. Met. Hard Mater. 33 93

[58] Meng J, Sun L, Zhang Y, Xue F, Chu C, Bai J 2020 Materials 13 427